Color Uniformity and Moire in Dispersed Dot Halftone Masks Generated by Linear Pixel Shuffling

Peter G. Anderson Jonathan S. Arney and Mark S. Guittard
Rochester Institute of Technology
Rochester, New York, USA

Abstract

We investigate a method for combining two dispersed-dot halftoning masks for two colors that generalizes the traditional angular displacement used with clustered-dot halftone screens.

Our masks were two variations of the Linear Pixel Shuffling algebraic mask algorithm involving numbers arising from two different third order, Fibonacci-like recurrences, As an alternative to screen rotation, these masks were repositioned by flipping and rotating, and all pairwise positional combinations of the transposed, inverted masks were used two at a time to generate cyan and magenta images, each at nominal dot fractions of 0.25. The resulting blue images were evaluated for color uniformity and moire using visual evaluations, Fourier analysis, and a color micro-variation analysis. This presentation will describe the analytical techniques used to evaluate color uniformity and moire.

1. Background: Dispersed Dot Halftoning Masks

The halftone mask method to convert a gray-scale image, *I*, to a bi-level image, *B*, employs a mask, *M*, as follows. Given a gray-scale image, *I*, of dimension *H* x *W*, we can use a mask *M*, of the same dimensions to convert *I* to a similar looking bi-level image *B* by the following rule:

$$B_{pq} = \begin{cases} 1, & \text{if } I_{pq} \geq M_{pq} \\ 0, & \text{if } I_{pq} < M_{pq} \end{cases} \quad (1)$$

In this form, we assume that the values of the image and of the mask are in the same range, typically 0–255 or 0.0–1.0. *M* can be constructed many ways. Roberts's methods simply uses pseudorandom numbers (white noise) and produces barely acceptable, mottled, bi-level images. B. Bayer introduced a method of constructing *M* in terms of replicated sub-windows or tiles.[3] R. Ulichney presents a wide variety of methods for constructing such tiles.[4]

We previously presented methods for creating masks based on third-order linear recurrences,[1,2] which we briefly review here. Two useful recurrences are the sequences referred to as $\mathcal{G}$ and $\mathcal{T}$ given by

$$G_0 = 0, \quad G_1 = G_2 = 1 \quad (2)$$

$$G_n = G_{n-1} + G_{n-3} \text{ for } n > 2 \quad (3)$$

$$T_0 = 0, \quad T_1 = T_2 = 1 \quad (4)$$

$$T_n = T_{n-1} + T_{n-2} + T_{n-3} \text{ for } n > 2 \quad (5)$$

$\mathcal{T}$ is known as the *Tribonacci sequence*, a generalization of the Fibonacci sequence. Let

$$A = S_n, \quad B = S_{n+1}, \quad C = S_{n+2} \quad (6)$$

where $\{S_n\}$ is either of our sequences. Define a mask, *M* by the rule

$$M_{pq} = (pA + qB)\%C \quad (7)$$

0	9	5	1	10	6	2	11	7	3	12	8	4
6	2	11	7	3	12	8	4	0	9	5	1	10
12	8	4	0	9	5	1	10	6	2	11	7	3
5	1	10	6	2	11	7	3	12	8	4	0	9
11	7	3	12	8	4	0	9	5	1	10	6	2
4	0	9	5	1	10	6	2	11	7	3	12	8
10	6	2	11	7	3	12	8	4	0	9	5	1
3	12	8	4	0	9	5	1	10	6	2	11	7
9	5	1	10	6	2	11	7	3	12	8	4	0
2	11	7	3	12	8	4	0	9	5	1	10	6
8	4	0	9	5	1	10	6	2	11	7	3	12
1	10	6	2	11	7	3	12	8	4	0	9	5
7	3	12	8	4	0	9	5	1	10	6	2	11

Figure 1. A tile of an algebraic mask for halftone mask with parameters A = 6, B = 9, C = 13.

This defines a mask with valued periodic in *p* and *q* with period *C* in both cases—that is a *C* x *C* tile—with the values {0, 1, …,C 1} each appearing *C* times in the tile. The latter observation is a consequence of

$$\gcd(S_n, S_{n+1}, S_{n+2}) = 1 \quad (8)$$

for both our sequences. Figure 1 shows the tile for $A = 6$, $B = 9$, $C = 13$. These masks are particularly convenient to use because each value can be computed from the value to its left or above it by an addition followed by a conditional subtraction—the table does not need to be stored. Figure 2 shows a gray-scale image rendered using the Tribonacci parameters $A = 81$, $B = 149$, $C = 274$.

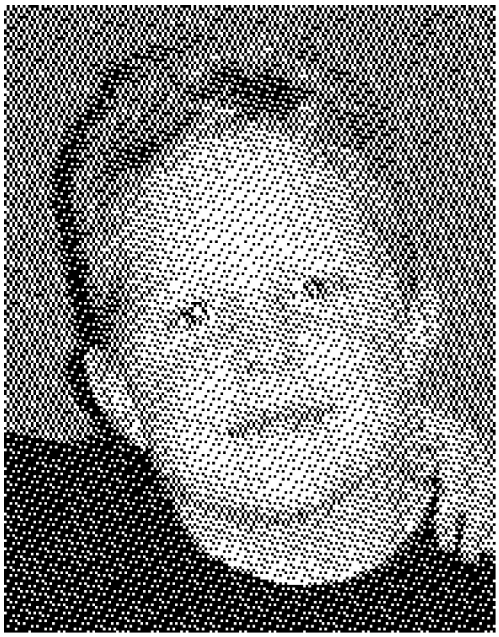

Figure 2. Image halftoned using the mask with the Tribonacci parameters A = 81, B = 149, C = 274.. This image is printed with "fat pixels" to show the dot patterns used and to avoid artifacts introduced by printing.

2. The Problem: Masks For Multiple Color Planes

Traditional printing uses clustered dots and rotates the masks for the different colors through angles relative to each other. This rotation avoids moire that might be introduced by a small misregistration of the color planes in the printed image or though a high correlation of the color levels in different planes. This rotation also achieves an independence of the printing of two colors, *A* and *B*, relative to each other. The area fraction of dots of color *A* that are painted over by ink of color *B* is simply the total area fraction of color *B* by itself. This avoids inadvertent color shifting that would occur from the two extreme situations: either printing color *B* totally on top of color *A*, or of color *A* completely missing color *B* areas.

How can we generalize algebraic masks to color printing to achieve what traditional printers achieve with rotated clustered dots patterns?

3. Experiments With Pairs of Algebraic Masks

Instead of rotating a mask relative to itself to apply to the various color planes, we create different masks by the operations of reflection and 90° rotations, that is, the eight symmetries of a square.

The eight symmetries of the masks are indicated by Table 1. For the T_0 mask, we used the parameters $A = 274$, $B = 504$, $C = 927$. For the G_0 mask, we used the parameters $A = 595$, $B = 872$, $C = 1278$.

Table 1. Nomenclature for the Symmetries of the $\mathcal{G}$ Masks

G_0	$\mathcal{G}$ mask in standard position
G_1	G_0 rotated 90° counter-clockwise
G_2	G_0 rotated 180° counter-clockwise
G_3	G_0 rotated 270° counter-clockwise
G_4	G_0 flipped top to bottom
G_5	G_4 rotated 90° counter-clockwise
G_6	G_4 rotated 180° counter-clockwise
G_7	G_4 rotated 270° counter-clockwise

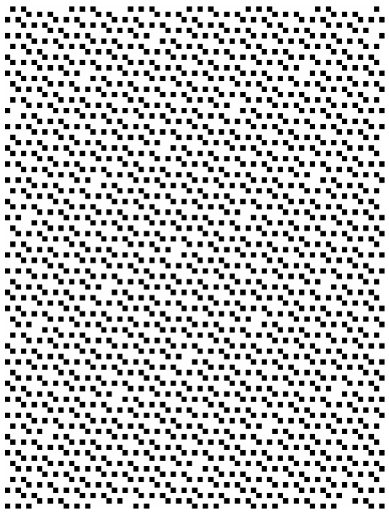

Figure 3. The dispersed dot pattern of a 25% gray image halftoned using the mask with the Tribonacci parameters A = 81, B = 149, C = 274.

We created images with color 25% cyan and 25% magenta using 7+7+8 = 22 pairs of masks, as follows:

$$\langle G_0, G_1\rangle, \cdots, \langle G_0, G_7\rangle$$
$$\langle T_0, T_1\rangle, \cdots, \langle T_0, T_7\rangle$$
$$\langle G_0, T_0\rangle, \cdots, \langle G_0, T_7\rangle$$

The pair $\langle M, M'\rangle$ would create the image of 25% cyan quantized using mask *M* and 25% magenta quantized using mask *M'*. We did not use any mask combined with itself for the reasons discussed above.

The 22 generated color images were evaluated with three methods:

1. Visual assessment of color uniformity.
2. Frequency composition (Fourier) analysis.
3. Box analysis to study the variation of the image in sampled sub-windows.

We used J programming language to generate the images. The results are summarized in Table 2.

3.1. Visual Assessment

Blue halftone images were simulated on a color CRT monitor by using cyan masks to control the red phosphors and magenta masks to control the green phosphors. The blue was always at 100% output. The simulated halftone dots were constructed as 1 mm. x 1 mm. dots. With a monitor screen resolution of six RGB dots per millimeter, the simulated halftone dots contained approximately 36 phosphor dots. Halftone dots representing cyan ink were displayed with the blue and green phosphors at 100% output and the red phosphor at 0% output. Similarly, the magenta halftone dots used red and blue phosphors with the green turned off, and blue halftone dots were formed with the blue phosphor only. A simulated blue halftone was generated in this way for each of the 22 combinations of masks described above.

The relative spatial uniformity of the simulated blue halftones were evaluated visually. Each blue halftone was displayed individually on the monitor. The authors could easily see the individual 1 mm. x 1 mm. dots of cyan, magenta, blue, and white at a viewing distance of 0.5 meter. The authors backed up to increase the viewing distance until the individual colors blended to a spatially uniform blue. The relative quality of the different mask combinations was used as the metric of relative color uniformity. The results are shown in the second column of Table 2.

3.2. Fourier Analysis

A noise power analysis was also applied to the blue halftone images as a means of estimating the relative spatial uniformity of the 22mask combinations. In this case the simulated halftone image was constructed within the computer by defining reflection spectra for the virtual paper (R_p = 1.00 for 400–700 nm); for the virtual cyan ink (R_c = 0.00 for 600–700 nm and 1.00 elsewhere); and for the virtual magenta ink (R_m = 0.004 for 500–600 nm and 1.00 elsewhere). The reflectance of the overlap blue was defined as 1.00 from 500 to 700 nm, and zero elsewhere. Each of the 22 mask combinations produced an array of colored dots of cyan, magenta, blue, and white.

The L*a*b* value for each pixel was calculated from the defined reflection spectrum of each pixel. The average reflectance spectrum for the image was calculated and the corresponding L*a*b* for the overall image determined. A color difference, ΔE, between the halftone dot and the overall image was calculated for each individual dot. The resulting matrix of ΔE values was a spatial distribution of color variation for the blue halftone. A variation matrix of this kind was determined for each of the 22 mask combinations, and 2D noise power spectra were calculated for each. Visual examination of the noise power spectra did not suggest a useful metric for comparison of relative color uniformity, but they did reveal more complex behavioral differences that will be basis for follow up analysis.

3.3. Box Analysis

This analysis of color uniformity was carried out in the spatial domain of the virtual color images described in part 3.2 above. An N x N aperture box was defined where N is the number of virtual halftone dots. The box was placed in the upper left hand corner of the virtual halftone, and additional boxes were placed in sequence to tile over the entire image. Within each box the average reflectance spectrum and the corresponding L*a*b* value was found. Then the standard deviation for each color coordinate was calculated, σ_L, σ_a, and σ_b, and the overall RMS color deviation for the image was determined:

$$\sigma_E = \left(\sigma_a^2 + \sigma_b^2\right)^{1/2} \tag{9}$$

The value of N was then increased and the analysis repeated to generate another value of σ_E. As anticipated, σ_E decreased as the aperture box size, N, increased. It was observed that σ_E increased linearly with $1/N$, and the following metrics of color variation were defined from these graphs. These three metrics of color variation are defined as follows, and their values for each of the 22 mask combinations are shown in Table 2.

(a) N_5 is the value of N for σ_E = 5. This corresponds to a color difference, σ_E, of 5, which is noticeable by most people but small. A value of 5 was used for comparison of the 22 mask combinations rather than the approximate JND of 1.0 because many of the mask combinations did not achieve σ_E = 1.

(b) $N_{\min}$ is the value of N at which σ_E = 0. Several mask combinations did not show a zero color deviation even as the box size went to infinity ($1/N$ = 0).

(c) $\sigma_{E\min}$ is the value of σ_E at $1/N$ = 0. This was included since even if a system did not have an $N_{\min}$, it would always have a minimum σ_E.

4. Observations and Conclusions

Examination of the four color uniformity metrics in Table 2 shows significant differences between the 22 mask combinations. Contrary to our initial expectations, there was very little correlation between the different metrics in Table 2. However, further consideration suggests this should not be surprising, as outlined below.

First, the visual distance metric, Dist., in column 2 of Table 2, varied only slightly among the 22 mask combinations, but the calculated metrics in columns 3, 4, and 5 varied much more. The box metrics, N_5 and $N_{\min}$ were specifically designed to mimic the visual distance metric. However, the spectrum of phosphors on the CRT monitor are quite different from the idealized spectra of the virtual

halftones on which the box metrics are based. In addition, the monitor resolution may tend to low-pass the simulated displayed halftone. The overall effect is that visual inspection of a synthetic halftone on a monitor appears not to be a very sensitive index of relative color uniformity, at least as done in this project. Further work is needed to develop a visual evaluation experiment to provide useful insights into the visual significance of color uniformity associated with different color halftone algorithms.

Table 2. Metrics for the cyan and magenta images generated from mask pairs.

Image	Dist.	N_5	N_{min}	σ_{Emin}
$<G_0G_1>$	15	13.7	1042	0
$<G_0G_2>$	16	19.1	133	0.021
$<G_0G_3>$	16	14.0	∞	0.196
$<G_0G_4>$	16	13.9	∞	0.111
$<G_0G_5>$	17	17.1	102	0
$<G_0G_6>$	15	13.6	∞	0.017
$<G_0G_7>$	16	18.4	214	0.203
$<G_0T_0>$	15	19.0	70	0
$<G_0T_1>$	14	13.2	98	0
$<G_0T_2>$	14	18.9	113	0
$<G_0T_3>$	16	12.6	132	0
$<G_0T_4>$	15	12.5	100	0
$<G_0T_5>$	14	19.0	84	0
$<G_0T_6>$	15	13.0	104	0
$<G_0T_7>$	15	18.9	131	0
$<T_0T_1>$	16	14.1	133	0
$<T_0T_2>$	15	18.0	103	0
$<T_0T_3>$	16	13.6	165	0
$<T_0T_4>$	16	13.4	251	0
$<T_0T_5>$	15	19.2	64	0
$<T_0T_6>$	16	14.0	177	0
$<T_0T_7>$	14	19.3	88	0

Among the three box metrics of color uniformity, the minimum color variation, σ_{min}, appears useful only as an index of the worst cases. The most color uniform mask combinations all were capable of a zero color variation at some box size, N. All of combinations with at least one of T_i type mask were capable of $\sigma_{min} = 0$, so further analysis was limited only to those 15 combinations.

The N_5 and N_{min} metrics were intended to be a simulation of an ideal visual distance experiment. In both cases, a smaller value indicates better color uniformity. However, the correlation between these two metrics is very low, and indeed the correlation coefficient is negative (r = -0.05) for the 15 combinations containing a $\mathcal{T}$ mask. Figure 4 shows the correlation. The absence of a positive correlation, coupled with the apparent bimodal distribution in Figure 4, suggests that a single color uniformity metric is insufficient to characterize the relative quality of spatial variations in color of the mask combinations.

This work has not resulted in a clear preference for a single number metric for comparison of color uniformity of different types of halftone algorithms. There may indeed be a single number metric, defined to correlate highly with appropriate visual preference experiments, but such a metric is clearly not a trivial matter to define. Nor is it trivial to define an appropriate experimental protocol for visual assessment of color uniformity capabilities of halftone algorithms. In particular, it is difficult to eliminate all artifacts associated with monitors. This work does show, however, that different color halftone algorithms do result in significant differences in color uniformity. Further work is being carried out develop better color halftone algorithms and to develop experimental protocols for their evaluation.

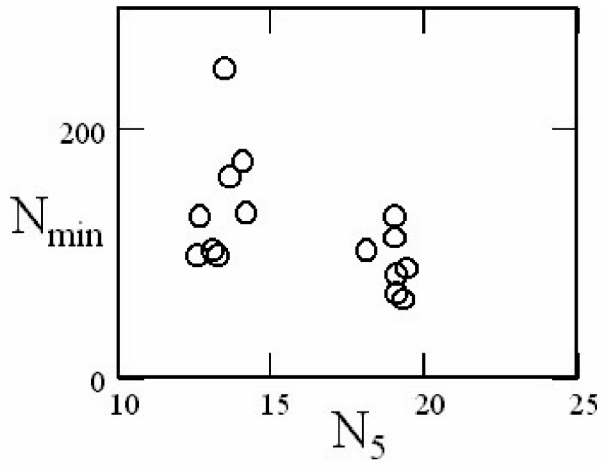

Figure 4. Nmin vs. N_5 for all mask combinations containing at least one $\mathcal{T}$ type mask.

References

1. Peter G. Anderson. An algebraic mask for halftone dithering. In Proceedings of the 47th Annual Conference of the Society for Imaging Science and Technology, pages 487–489, 1994.
2. Peter G. Anderson, Jonathan Arney, and Kevin Ayer. Linear pixel shuffling (I): New paradigms for new printers. In Proceedings of The 16th International Congress on Digital Printing Technologies (NIP 16), Springfield, VA, 2000. The Society for Imaging Science & Technology.
3. B. E. Bayer. An optimum method for two-level rendition of continuous-tone pictures. IEEE International Conference on Communications, 1:26–11, 26–15, 1973.
4. Robert Ulichney. Digital Halftoning. The MIT Press, 1987.

This research was supported by a grant from Hewlett-Packard.